Cell Reports
Article

Local Nucleosome Dynamics Facilitate Chromatin Accessibility in Living Mammalian Cells

Saera Hihara,[1,2,11] Chan-Gi Pack,[3,6,11] Kazunari Kaizu,[8,11] Tomomi Tani,[7,12] Tomo Hanafusa,[1] Tadasu Nozaki,[1,9] Satoko Takemoto,[4] Tomohiko Yoshimi,[10] Hideo Yokota,[4] Naoko Imamoto,[5] Yasushi Sako,[3] Masataka Kinjo,[6] Koichi Takahashi,[8,9] Takeharu Nagai,[7,13] and Kazuhiro Maeshima[1,2,5,*]
[1]Biological Macromolecules Laboratory, Structural Biology Center, National Institute of Genetics
[2]Department of Genetics, School of Life Science, Graduate University for Advanced Studies (Sokendai)
Mishima, Shizuoka 411-8540, Japan
[3]Cellular Informatics Laboratory
[4]Bio-research Infrastructure Construction Team
[5]Cellular Dynamics Laboratory
RIKEN Advanced Science Institute, Wako, Saitama 351- 0198, Japan
[6]Laboratory of Molecular Cell Dynamics
[7]Research Institute for Electronic Science
Hokkaido University, Sapporo 001-0021, Japan
[8]Laboratory for Biochemical Simulation, RIKEN Quantitative Biology Center, Suita, Osaka 565-0874, Japan
[9]Institute for Advanced Biosciences, Keio University, Fujisawa 252-8520, Japan
[10]Department of Bioengineering, Graduate School of Engineering Osaka City University, Osaka 558-8585, Japan
[11]These authors contributed equally to this work
[12]Present address: Cellular Dynamics Program, Marine Biological Laboratory, Woods Hole, MA 02543, USA
[13]Present address: The Institute of Scientific and Industrial Research, Osaka University, Ibaraki, Osaka 567-0047, Japan
*Correspondence: kmaeshim@nig.ac.jp
http://dx.doi.org/10.1016/j.celrep.2012.11.008

SUMMARY

Genome information, which is three-dimensionally organized within cells as chromatin, is searched and read by various proteins for diverse cell functions. Although how the protein factors find their targets remains unclear, the dynamic and flexible nature of chromatin is likely crucial. Using a combined approach of fluorescence correlation spectroscopy, single-nucleosome imaging, and Monte Carlo computer simulations, we demonstrate local chromatin dynamics in living mammalian cells. We show that similar to interphase chromatin, dense mitotic chromosomes also have considerable chromatin accessibility. For both interphase and mitotic chromatin, we observed local fluctuation of individual nucleosomes ($\sim$50 nm movement/30 ms), which is caused by confined Brownian motion. Inhibition of these local dynamics by crosslinking impaired accessibility in the dense chromatin regions. Our findings show that local nucleosome dynamics drive chromatin accessibility. We propose that this local nucleosome fluctuation is the basis for scanning genome information.

INTRODUCTION

The long string of genomic DNA must be organized three dimensionally in nuclei or mitotic chromosomes so as to utilize genome information during cellular proliferation, differentiation, and development. DNA is wrapped around histones, forming a nucleosome structure (Olins and Olins, 1974; Woodcock et al., 1976; Kornberg, 1974). The nucleosome is thought to be folded into a 30 nm chromatin fiber (Finch and Klug, 1976; Woodcock et al., 1984) and further regular higher-order structures (Sedat and Manuelidis, 1978; Belmont et al., 1987). However, recent analyses, including our cryo-electron microscopy (cryo-EM) and synchrotron X-ray scattering studies, showed almost no visible 30 nm chromatin fibers or other regular structures in mitotic chromosomes (McDowall et al., 1986; Eltsov et al., 2008; Maeshima et al., 2010a; Nishino et al., 2012), which suggests that chromosomes consist of irregular folding of nucleosome fibers, with a fractal organization, i.e., a polymer melt-like structure. More recently, the absence of 30 nm chromatin fibers in the majority of active interphase cells was also suggested (Maeshima et al., 2010a; Fussner et al., 2011a, 2011b; Joti et al., 2012).

The concept of a polymer melt-like structure implies that the nucleosome fibers may be constantly moving and rearranging at the local level, actions that are likely to be crucial for various genome functions (Dubochet et al., 1986; McDowall et al., 1986; Eltsov et al., 2008; Maeshima et al., 2010a; Nishino et al., 2012; Joti et al., 2012). Although many studies have examined chromatin dynamics on relatively long timescales, from seconds to hours (Abney et al., 1997; Vazquez et al., 2001; Heun et al., 2001; Zink et al., 2003; Soutoglou and Misteli, 2007; Chuang and Belmont, 2007; Bancaud et al., 2009; Cremer et al., 2012; McNally, 2011), much less is known about local nucleosome dynamics on a shorter timescale, from milliseconds to seconds. Here, we analyzed the local dynamic properties of nucleosome fibers in living mammalian cells.

Because studying the chromatin environment in living cells using traditional fluorescence and EM is difficult, we utilized

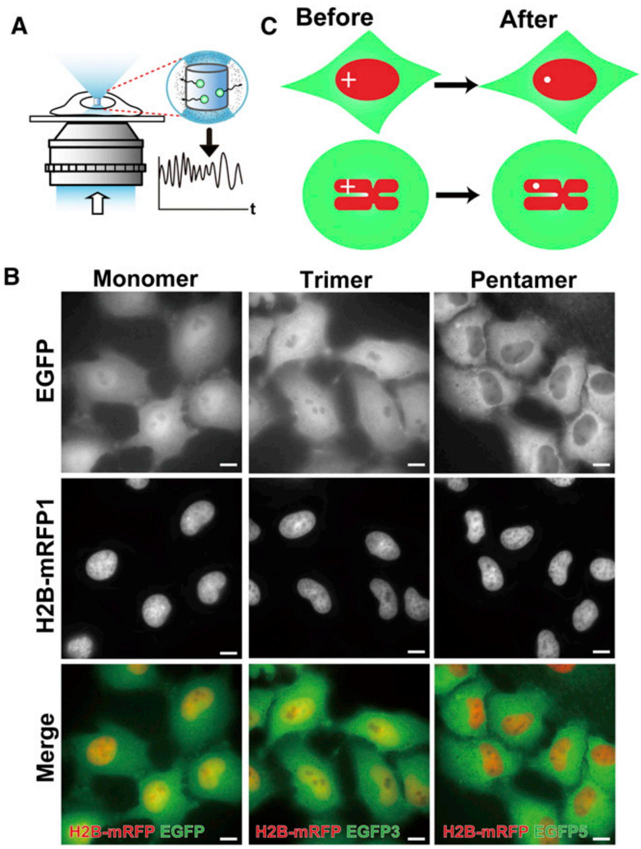

Figure 1. FCS Measurements in Living Cells

(A) Schematic diagram of FCS measurement. FCS detects the in-out motion of EGFP molecules (green spheres) in an ~0.1 femtoliter volume (the blue cylinder region) as fluctuations in fluorescence intensity (shown as a graph). t, time.

(B) DM cell lines that express the monomeric, trimeric, and pentameric forms of EGFP. First row shows EGFP signal; second row, H2B-mRFP1; third row, merged images. Note that the EGFP monomer and trimer are uniformly distributed in the cytoplasm and nuclei. The pentamer signal in the nuclei is also uniform, although its signal is weaker than that in the cytoplasm, probably because the pentamers cannot pass through the nuclear pores. Scale bars, 10 μm.

(C) Identification of FCS-measured regions. After FCS, the chromatin regions (H2B-mRFP1, red) are photobleached, and the actual measured regions (white circles) can be identified in the interphase chromatin (upper right) and mitotic chromosomes (lower right).

See also Figure S1.

a combined approach of fluorescence correlation spectroscopy (FCS), single-molecule imaging, and Monte Carlo computer simulations. FCS detects fluorescence intensity fluctuations caused by Brownian motion of fluorescence probe molecules in a small detection volume generated by confocal microscopic illumination (Rigler and Elson, 2001; Mütze et al., 2011). Using this approach, we can indirectly examine the cellular environment in living cells. Single-molecule imaging can directly reveal the dynamics of specific molecules (Harms et al., 2001; Schütz et al., 2000; Sako et al., 2000; for single-particle analysis, see Gross and Webb, 1986; Sheetz et al., 1989; Kues et al., 2001; Marshall et al., 1997). Computer simulation enables us to predict the behavior of molecules under conditions that are either difficult to observe directly by microscopic strategies or difficult to generate experimentally. Many simulations have been performed for polymers, DNA, nucleosomes, and chromatin, contributing to the understanding of chromatin structure and function (Schlick et al., 2012; Perišić et al., 2010; Fritsch and Langowski, 2010, 2011; Diesinger et al., 2010; Vologodskii and Rybenkov, 2009; Korolev et al., 2012; Becker and Everaers, 2009). To reconstruct the chromatin environment in living cells, we employed a type of Metropolis Monte Carlo simulation that solves particle diffusion problems (Metropolis et al., 1953; Morelli and ten Wolde, 2008).

In the present study using our combined approach, we uncovered the local dynamics of individual nucleosomes in living mammalian cells. Our results show that nucleosome fluctuation drives chromatin accessibility, which is advantageous for many "target searching" biological processes, including transcription, DNA repair, replication, and recombination.

RESULTS

FCS Measurements of Interphase Chromatin and Mitotic Chromosomes in Living Cells

To characterize chromatin accessibility in living cells, we first employed FCS using free enhanced green fluorescent proteins (EGFPs). Through time correlation analyses of the fluorescence fluctuations (Figure 1A), we obtained a diffusion coefficient (*D*) for free EGFP, which shows how far the molecules can move in a particular period of time (see Experimental Procedures; also see Figures S1 and S2). *D* provides useful information on their environment: a crowded environment decreases *D*.

However, we experienced two problems with FCS measurements, particularly in the mitotic chromosome environment. First, the diameter of the FCS detection regions (which are ~0.4 μm in diameter × ~1–2 μm in height) is larger than the diameter of a typical mammalian chromosome (~0.7 μm; Alberts et al., 2008), which makes specific measurements inside chromosomes difficult. Second, because chromosomes move dynamically and a single FCS measurement takes more than several seconds, we have to confirm that the measured region is actually inside the dynamic chromosomes throughout the recording period. To resolve the first problem, we used an Indian Muntjac cell line (DM cells) (Manders et al., 1999). DM cells have giant chromosomes with diameters that are much larger (~2 μm) than that of the FCS detection region. For the second problem, histone H2B-mRFP1 was coexpressed as a marker of chromatin regions (Pack et al., 2006; Dross et al., 2009; Bancaud et al., 2009) (Figures 1B, S1A, and S1B). Upon photobleaching of immobilized H2B-mRFP1 after FCS, the actual measured regions could be identified by confocal imaging, thus avoiding off-target measurements (Figures 1C, S1C, and S1D).

To establish DM cell lines that stably express H2B-mRFP1 and EGFP, we introduced a single-copy construct into the DM cell genome by site-specific recombination (Figure S1A). To examine the effect of the size of molecules on diffusion, we also generated DM cell lines that express oligomeric EGFPs: EGFP trimers and pentamers with molecular masses of 90 and

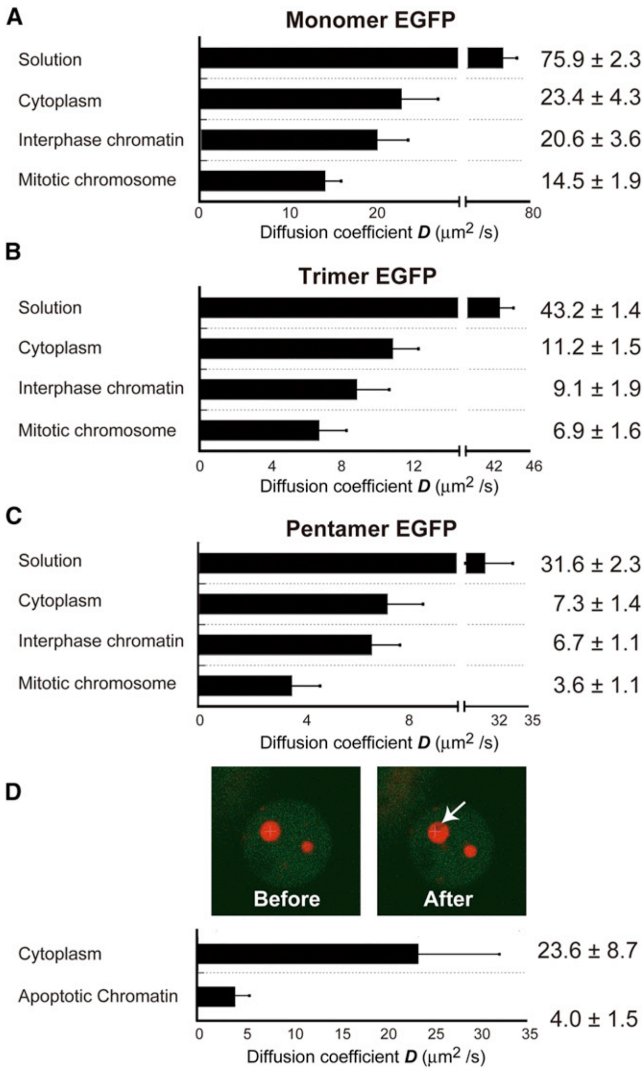

Figure 2. Mean *D* Values of EGFP Monomers, Trimers, and Pentamers in Living Cells

(A–C) EGF monomer (A), trimer (B), and pentamer (C) in solution (first row) (Pack et al., 2006) and cytoplasm (second row), interphase chromatin (third row), and mitotic chromosomes (fourth row) are shown. For details regarding the calculation of *D*, see Experimental Procedures. The mean value and SD are shown on the right (n = 5 cells).

(D) Slower diffusion of EGFP monomers in apoptotic chromatin. Upper view shows that the chromatin of apoptotic cells is condensed with a strong H2B-mRFP1 signal. After the FCS measurement, the H2B-mRFP1 signal of the measured region was photobleached (indicated by arrow). Lower view presents mean *D* values of EGFP monomers in the apoptotic cell cytoplasm and chromatin. Note that the value for the cytoplasm is similar to that of the cytoplasm of normal cells. The *D* value in the apoptotic chromatin was 3-fold lower than mitotic chromosomes, whereas the cytoplasm of interphase, mitotic, and apoptotic cells did not show such low *D*s. Thus, although both are highly condensed, the compaction profiles of mitotic and apoptotic chromatin appear to be distinct, suggesting that the nucleosomes in "dying cells" were aggregated and their local movement diminished, different from those in living cells.

See also Figure S2.

150 kDa, respectively (Figures 1B and S1B; for details of the construction of the oligomeric EGFPs, see Extended Experimental Procedures). The oligomeric EGFPs with different molecular masses could be used as molecular rulers for quantifying protein mobility (Pack et al., 2006; Dross et al., 2009; Bancaud et al., 2009). Their proper expression and localization were confirmed by microscopic imaging (Figure 1B) and western blotting (Figure S1B).

Interphase Chromatin and Mitotic Chromosomes Have Considerable Chromatin Accessibility

We then measured the movements of the EGFP monomer, trimer, and pentamer molecules in the interphase chromatin and mitotic chromosomes (Figure 1A; Experimental Procedures). Before and after the FCS measurements, cell images were acquired to verify the actual measured regions by photobleaching of H2B-mRFP1 (Figures S1C and S1D). Based on the measured fluorescence correlation functions, which were well fitted by the one-component model, we calculated the *D*s of EGFP monomer, trimer, and pentamer molecules (Figure S2; Experimental Procedures). Figure 2A shows the *D*s of monomer EGFP molecules in the cytoplasm, interphase chromatin, and mitotic chromosomes. The *D*s obtained for the cytoplasm and interphase chromatin are similar to those in previous reports (Pack et al., 2006; Dross et al., 2009; Bancaud et al., 2009). In the mitotic chromosome, protein mobility or accessibility was detected, as implied by other studies (Chen et al., 2005; Hinde et al., 2011; Görisch et al., 2005). The *D* in the mitotic chromosomes was only 30% lower than that in the interphase chromatin. Similar profiles for the EGFP trimers and pentamers were observed (Figures 2B and 2C). Our results show that similar to interphase chromatin, mitotic chromosomes also have considerable chromatin accessibility. However, we found that EGFP mobility was severely impaired in apoptotic chromatin, which is highly condensed (Figure 2D), suggesting that the comparable *D*s in interphase chromatin and mitotic chromosomes were not due to our FCS measurement system (see also Figure 2D legend).

Nucleosome Concentrations within Interphase Nuclei and Mitotic Chromosomes in DM cells

We did not detect large differences in chromatin accessibility between interphase chromatin and mitotic chromosomes. Therefore, to more directly evaluate their chromatin environment, we examined the nucleosome concentrations in interphase nuclei and mitotic chromosomes. Nuclear and mitotic chromosome volumes in DM cells were measured from their three-dimensional (3D) image stacks (Figures 3A and 3B). Their nucleosome concentrations were calculated based on the measured volumes and the known genome size of Indian Muntjac cells (DM cells) (2.1 pg/haploid genome) (Johnston et al., 1982). The nucleosome concentration in mitotic chromosomes (~0.5 mM) was 5-fold higher than that in interphase nuclei (~0.1 mM) (Figure 3C), which is consistent with previous reports (for fluorescence-based measurements, see Weidemann et al., 2003; for EM-based measurements, see Daban, 2003), although one must consider that nucleosomes are not evenly distributed within interphase nuclei.

Cell PRESS
Open ACCESS

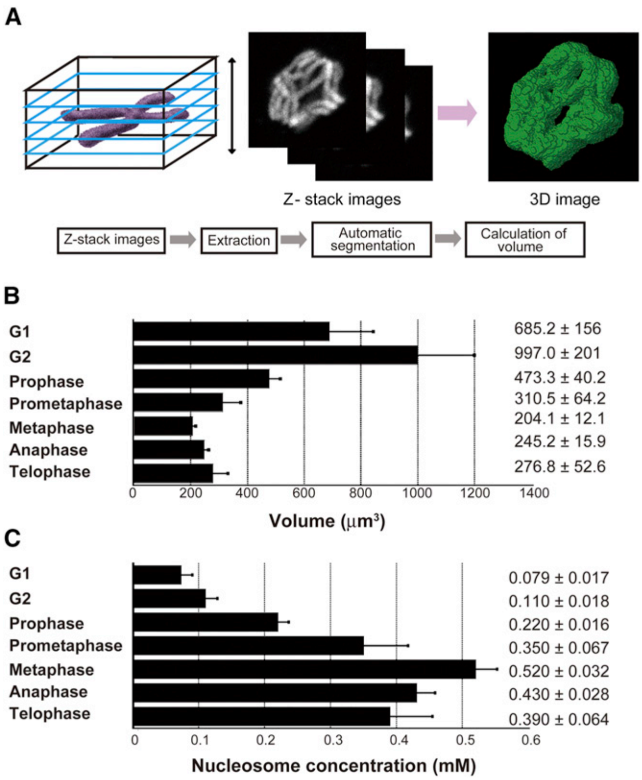

Figure 3. Measurements of Nucleosome Concentrations in Interphase Nuclei and Mitotic Chromosomes

(A) Chromatin regions were extracted and segmented from the 3D image stacks through the use of an extraction and segmentation procedure (left two images; for details, see Extended Experimental Procedures). The nuclear and chromosome volumes were calculated from the segmented areas. Note that because the chromosome clusters, especially in anaphase, have complicated shapes, the chromosome volumes may have been underestimated.

(B and C) The obtained volumes (B) and concentrations (C) are shown as bar graphs (left), and their mean values and SD are shown on the right (n = 4 cells).

In Silico Reconstruction of the Chromatin Environment Predicts that Nucleosome Fluctuation Facilitates Protein Mobility

Based on the physical parameters obtained above, we reconstructed the chromatin environment in silico using the Metropolis Monte Carlo method (Metropolis et al., 1953; Morelli and ten Wolde, 2008) to simulate EGFP behavior under various chromatin conditions. In the simulation, EGFP pentamers and the nucleosomes were represented as diffusing spherical particles of 13 nm hydrodynamic diameter (termed 13 nm spheres or green spheres in Figure 4A) and immobile spherical particles of 10 nm hydrodynamic diameter (termed 10 nm spheres or red spheres in Figure 4A), respectively. The hydrodynamic diameters of the particles were determined based on the Stokes-Einstein relation (for details, see Experimental Procedures). The 10 nm spheres, which mimic nucleosomes, were placed in the simulation volume at a concentration of 0.1 or 0.5 mM (red spheres in Figure 4A). The 0.5 mM condition corresponds to mitotic chromosomes and likely corresponds to interphase heterochromatin (Weidemann et al., 2003; Daban, 2003; for review, see Wachsmuth et al., 2008). In the environment with 0.1 mM of the 10 nm spheres (red spheres) under a fixed condition, the 13 nm spheres (green spheres) moved around freely (Figures 4B, left, and 4E; Movie S1). However, with the 0.5 mM fixed 10 nm spheres, which corresponds to the dense heterochromatin or chromosome environment, the 13 nm spheres could not move far from their starting position and were trapped in a confined space (Figures 4B, right, and 4E; Movie S2). The mean-square displacement (MSD) and *D*s of the 13 nm spheres under this condition are plotted in Figure S3. This simulation suggests that EGFP pentamers in fixed chromatin environments cannot move around freely. This is inconsistent with the FCS measurements in the living chromatin environment, in which apparently free diffusion of EGFP pentamers was observed.

To determine the conditions that better recapitulate the observations in vivo, we next performed the simulation with mobile nucleosomes. In this model, the 10 nm spheres (nucleosomes) are mobile, but their movements are restricted to a certain range, resembling "a dog on a leash" situation. In this dynamic environment, apparently free diffusion of the 13 nm spheres (green spheres) was observed with 0.5 mM of the 10 nm spheres (red spheres) (Figures 4C and 4E; Movie S3). The MSD and *D*s of the 13 nm spheres under this condition are plotted in Figure S3. This result suggests that in a dynamic chromatin environment, EGFP pentamers can move freely, even with 0.5 mM nucleosomes. In addition to the 13 nm spheres, we also showed that 21 nm spheres, which are twice as large as the nucleosome, can move freely in 0.5 mM of fluctuating 10 nm spheres (Figures S4A–S4C; Discussion).

Strikingly, a maximum displacement (or fluctuation) of 10–20 nm for the 10 nm spheres was sufficient for the 13 nm spheres to diffuse freely in the crowded environment (Figure 4D). This observation suggests that local fluctuation (10–20 nm) of nucleosomes drastically increases protein mobility in a compact chromatin environment. Furthermore, in the relatively low concentration range of 0.1–0.4 mM of 10 nm spheres, local fluctuation facilitated movement of the 13 nm spheres (Figure 4E), which agrees with the lattice simulations of the polymer chain (Wedemeier et al., 2009b; Fritsch and Langowski, 2011), whereas fluctuation of the 10 nm spheres at a higher concentration had a much greater effect (Figure 4E).

In our Monte Carlo simulation, we assumed that EGFP pentamer molecules were globular shapes with a hydrodynamic diameter of 13 nm. When we conducted additional calculations assuming the EGFP pentamer as a rod-shaped object, consistent results were obtained (Figures S4D–S4F).

Single-Nucleosome Imaging in Living Cells

An obvious important question is whether the nucleosome fluctuations predicted by the simulation occur in living cells. Therefore, we performed single-particle imaging of nucleosomes in living cells. Fluorescently labeling only a small number of the nucleosomes among the $\sim 3 \times 10^7$ in a single nucleus was technically challenging. We fused photoactivatable (PA)-GFP with histone H4 (Lippincott-Schwartz and Patterson, 2009; Wiesmeijer et al., 2008), which is a stable core histone

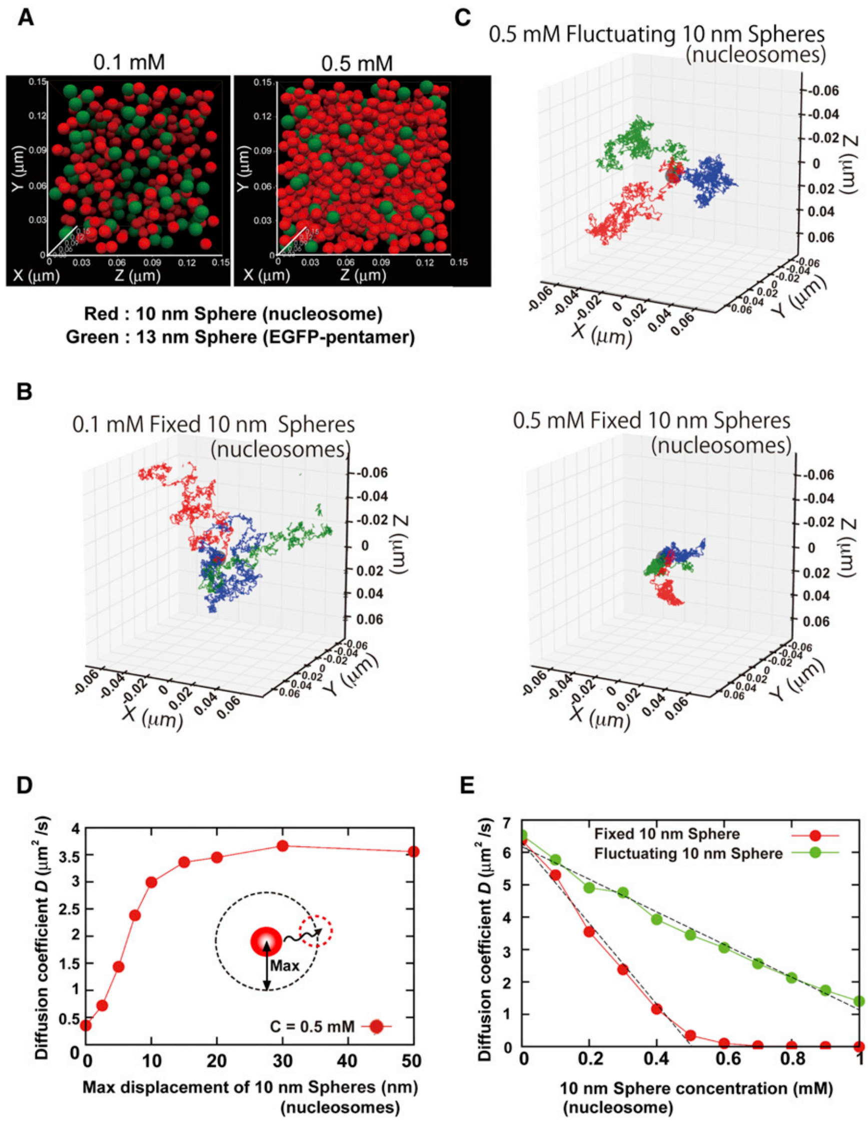

Figure 4. Reconstructions of the Living Chromatin Environment Using Monte Carlo Computer Simulations

(A) The nucleosome is represented as a 10 nm sphere (red sphere) and fixed in a restricted space at a concentration of 0.1 mM (left image) or 0.5 mM (right image, corresponding to mitotic chromatin or interphase heterochromatin), randomly but in a manner that avoids any overlap. The EGFP pentamer is represented as a 13 nm sphere (green sphere) (Pack et al., 2006; Wachsmuth et al., 2008) (also see Experimental Procedures).

(B) The 13 nm spheres (EGFP pentamers) are put in random motion, avoiding the 10 nm spheres (nucleosomes) at the obtained *D* (7.0 $\mu m^2/s$). With 0.1 mM of fixed 10 nm spheres, the 13 nm spheres move around freely (left image). However, with 0.5 mM of fixed 10 nm spheres, the 13 nm spheres are unable to move far from their starting points (right image). The three different temporal trajectories of the 13 nm spheres for 0.2 ms are indicated in blue, green, and red.

(C) In the environment with fluctuation of 0.5 mM of the 10 nm spheres, the 13 nm spheres can move around freely, in contrast to the case of fixed 10 nm spheres (right in B). Each 10 nm sphere behaves like "a dog on a leash." The leash length is 20 nm.

(D) Terminal *D*s of the 13 nm spheres with 0.5 mM of 10 nm spheres and various "dog leash" lengths (maximum displacement of 10 nm spheres). Note that a 10–20 nm displacement (movement) of the 10 nm spheres allows 13 nm spheres to diffuse quite freely.

(E) Terminal *D*s of 13 nm spheres with various 10 nm spheres concentrations, which are fixed (red) or fluctuating (green). Note that, in the relatively low concentration range of 0.1–0.4 mM of 10 nm spheres, local fluctuation facilitated movement of the 13 nm spheres. The "dog leash" (maximum 10 nm sphere displacement [movement]) length is 20 nm.

See also Figures S3 and S4 and Movies S1, S2, and S3.

component (for analyses using Histone-GFP, see Kimura and Cook, 2001), and expressed the fusion protein in DM cells at a very low level. PA-GFP-H4 expression and photoactivation in stable DM cells were verified using western blotting (Figure S5A) and 405 nm laser stimulation (Figure S5B), respectively. Biochemical fractionation of purified bulk nucleosomes confirmed that ectopically expressed PA-GFP-H4 behaved in a manner similar to endogenous H4, and the majority of PA-GFP-H4 was properly incorporated into the nucleosome structure (Figure S5C).

For single-nucleosome imaging, we used highly inclined and laminated optical sheet (HILO) microscopy (Tokunaga et al., 2008). Unexpectedly, a very low number of PA-GFP-H4 in the stable DM cells were spontaneously activated without laser activation and were observed as dots (Figure 5A). Single-step photobleaching of these dots (Figure 5B) revealed that each dot represented a single PA-GFP-H4 molecule in a single nucleosome, allowing one to observe the movement of individual nucleosomes.

Local Nucleosome Fluctuation in Living Cells

With this imaging system, we recorded nucleosome signals in the interphase chromatin and mitotic chromosomes at a video rate of ~30 ms/frame, as a movie. The signal particles in each image frame were fitted to an assumed Gaussian point spread function to determine the precise center of signals with a higher resolution below the diffraction limit (Figure 5A) (Lippincott-Schwartz and Patterson, 2009). After the position of the signal particles was obtained in every frame of the movie, its trajectory was analyzed as the displacement (movement) (Figures 5C and 5D). Because we aimed to examine local nucleosome fluctuations and the PA-GFP-H4s were very rapidly photobleached, we were able to analyze the behaviors of the nucleosomes over short time periods; from 0 to 0.18 s (Figures 5C, 5D, and 6).

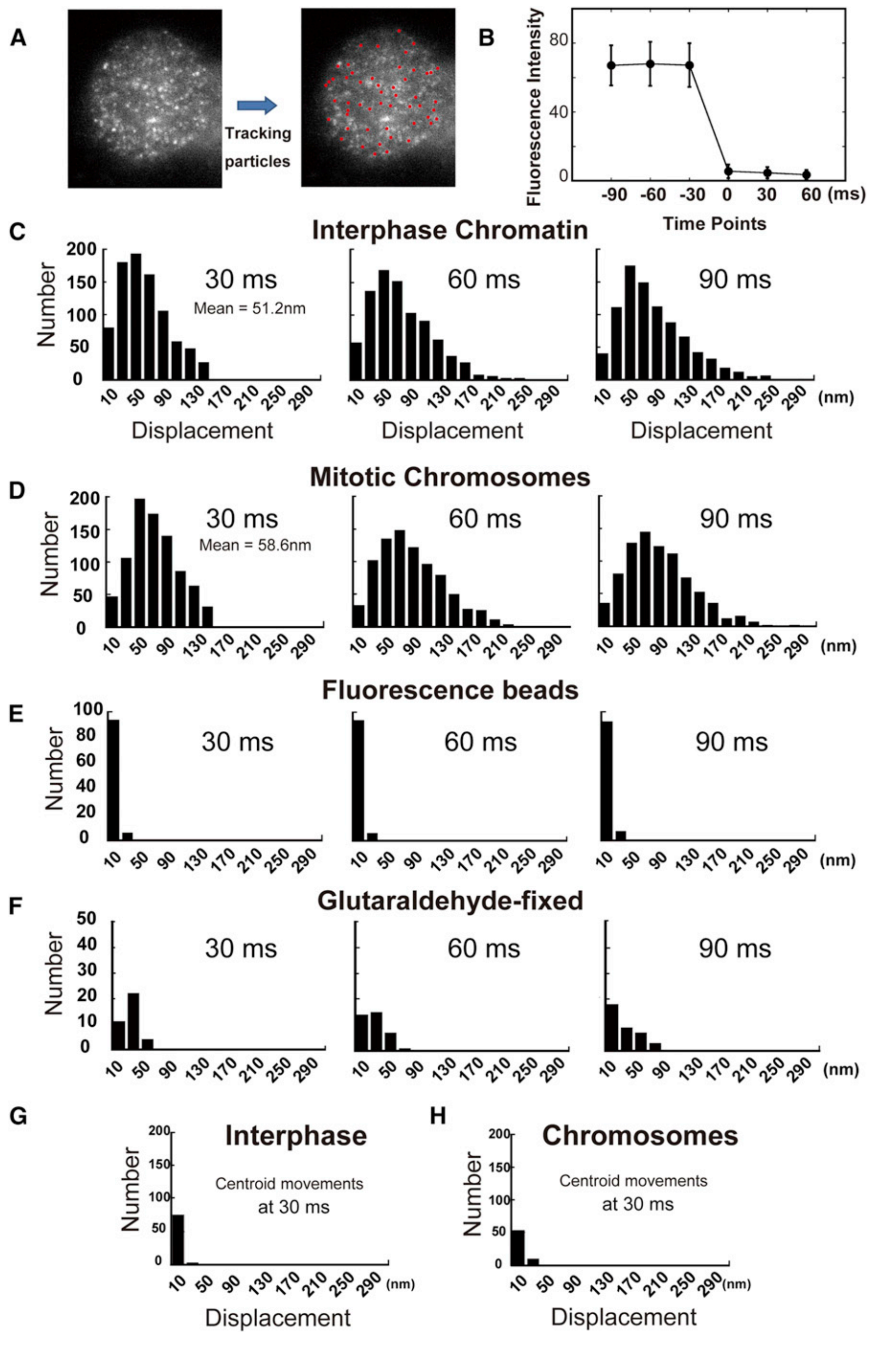

Figure 5. Single-Nucleosome Analysis

(A) Images of DM cell nuclei that express PA-GFP-H4. The bright dots are shown using the HILO microscopy system (Tokunaga et al., 2008) (for details, see Experimental Procedures).

(B) Single-step photobleaching of PA-GFP-H4 dots. The vertical axis represents the fluorescence intensity of each tracked PA-GFP-H4 dot. The horizontal axis is the tracking time series (photobleaching point is set as time 0; n = 100). Due to the clear single-step photobleaching profile of the PA-GFP-H4 dots, each dot in (A) shows a single PA-GFP-H4 molecule in a single nucleosome.

(C and D) Displacement (movement) distributions of single nucleosomes in interphase chromatin (C) (n = 8 cells) and mitotic chromosomes (D) (n = 12 cells) for 30 ms (left), 60 ms (center), and 90 ms (right).

(E) Displacement distributions of single fluorescence beads on a glass surface (n = 100).

(F) Crosslinked nucleosomes in glutaraldehyde-fixed DM cells (n = 8 cells). The glutaraldehyde-fixed cells produced strong autofluorescence, preventing determination of the signal centers. Note that their displacements are significantly less than in living cells (C) and (D).

(G and H) Centroid movements for many dots in the same time frame. Note that the centroid movements are much smaller than those in (C) and (D), suggesting that the detected nucleosome movement is not derived from the global motion of nuclei or chromosomes.

See also Figures S5, S6, and S7.

Figures 5C and 5D show the displacement distribution of single nucleosomes in living interphase and mitotic cells. The averaged displacements during 30 ms in the interphase chromatin and mitotic chromosomes were 51 and 59 nm, respectively. Because the displacements of fluorescent beads on the glass surface or the crosslinked nucleosomes in the glutaraldehyde-fixed cells were much smaller than those observed in living cells (Figures 5E and 5F), the results indicate that the majority of the displacement came from movement of nucleosomes in living cells, and not from drift in the microscopy system. To exclude further the possibility that the detected movement was derived from global motion of the nuclei or chromosomes, the movements of the centroid for nucleosomes were measured and plotted (Figures 5G and 5H). Because these values were much lower than the movements of individual nucleosomes in living cells (Figures 5C and 5D), we conclude that the observed displacement is due to local fluctuation of nucleosomes in living cells. In addition to the measurements using DM cells, we found that HeLa cells expressing a low level of PA-GFP-H4 also showed considerable nucleosome mobility (Figure S6), which suggests that local nucleosome movement in mammalian cells is a general phenomenon.

Local Nucleosome Fluctuation Is a Restricted Movement

To further analyze local nucleosome movement in DM cells, the MSD values (μm^2) of the nucleosomes in the interphase chromatin and mitotic chromosomes were plotted (Figure 6). The plots fitted well with the exponential equation MSD = $0.021t^{0.37}$ for interphase chromatin and with MSD = $0.018t^{0.31}$

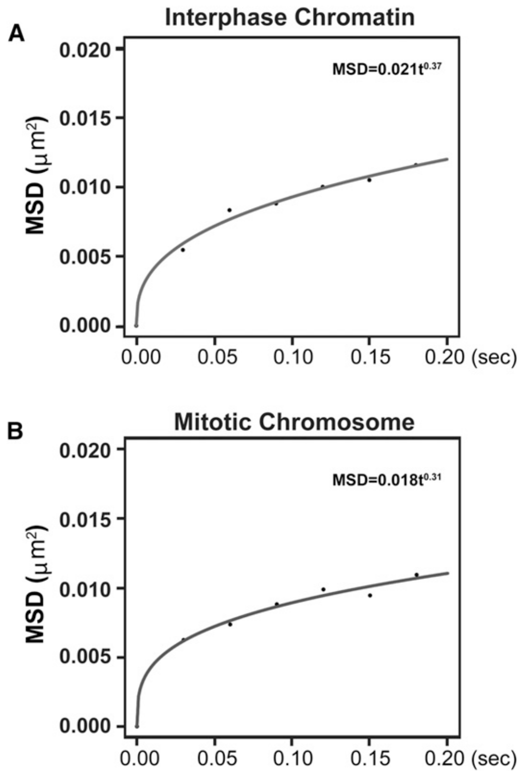

Figure 6. Plots of the MSDs of Single Nucleosomes from 0 to 0.18 s in Interphase Chromatin and Mitotic Chromosomes

Fluorescent bead data (Figure 5E) were used as the background. The plots were fitted as an anomalous diffusion, suggesting that the nucleosome movement supports a restricted diffusion model.

See also Figures S5, S6, and S7.

for mitotic chromosomes, respectively (Figure 6). The MSD values increased rapidly, and the slope decreased over time, supporting the restricted nucleosome movement model (see Discussion).

Formaldehyde-Fixed Cells Show Considerable Nucleosome Mobility

When we fixed the cells with formaldehyde, which less frequently crosslinks the same amino acid residues (predominantly arginine and lysine) than glutaraldehyde (Griffiths et al., 1993), we found that the cells still showed considerable nucleosome mobility (Figure S7). This result implies that the local nucleosome movement is caused by Brownian motion.

Inhibition of Local Nucleosome Dynamics Impairs Chromatin Accessibility in Dense Chromatin Regions

We next examined whether local dynamics are required for chromatin accessibility or targeting in the dense chromatin regions. For this purpose, we used condensin immunostaining (Hirano, 2005) as a probe for dense chromatin regions. Condensin localizes inside mitotic chromosomes like axes (Hirano, 2005). The immunostaining signals demonstrated that the antibodies (150 kDa, >15 nm) (Sandin et al., 2004) target the condensin inside the chromosomes (Figure 7A). We detected antibody signals in the chromosome axes of unfixed and formaldehyde-fixed cells, although much less staining was observed in the glutaraldehyde-fixed cells (Figures 7B and 7C). We also obtained a similar result using the H4K8-acetyl antibody (Figure 7D). These results show that tight crosslinking of nucleosomes blocks antibody accessibility and targeting. Consistently, we observed local nucleosome fluctuation both in living cells and formaldehyde-fixed cells (Figures 5C, 5D, and S7A), but not in glutaraldehyde-fixed cells (Figure 5F). Because we readily detected the antibody signals in the glutaraldehyde-fixed cell lysates by western blotting (Figure 7E), glutaraldehyde was unlikely to have changed the antibody-epitope(s) and prevented antibody access. This finding supports the idea that local nucleosome movement is important for chromatin accessibility and targeting in dense chromatin regions.

DISCUSSION

We used a combined in vivo/in silico strategy to study chromatin fluctuations, involving FCS measurements in the chromatin environment, reconstruction of chromatin environment using Monte Carlo computer simulations, and direct imaging of single-nucleosome dynamics. The combined approach demonstrated that nucleosome fluctuation facilitates chromatin accessibility in living mammalian cells. Notably, nucleosome fluctuation affects condensed chromatin environments as well as rather dilute environments, such as interphase chromatin.

It is reasonable to discuss the consistency between the in vivo/in silico experiments. Single-nucleosome imaging indicated a restricted movement of the nucleosome. This implies that nucleosomes can move freely and rapidly in certain restricted areas, which agrees with the fact that linker DNA connects nucleosomes to one another. We mimicked this situation using the "dog on a leash" model in our simulations. The "leash" restricts the movement of the 10 nm spheres (nucleosomes). The simulation results suggested that 10–20 nm fluctuations of 10 nm spheres (nucleosomes) drastically increases the mobility of the 13 nm spheres (EGFP pentamers) in the environment. The 10–20 nm leash length seems to be reasonable because normal linker DNA is 20–60 bp long, corresponding to a distance of 6.6–20.4 nm (0.33 nm/bp). In the simulation model, to complete the 20 nm movement, the 10 nm spheres (nucleosomes) required an average of 8.21 μs. According to the formula ($MSD = 0.018t^{0.31}$) from the single-nucleosome imaging, the nucleosome moves 21.8 nm in 8.21 μs, revealing consistency between the simulation and single-nucleosome imaging results.

Recent studies, including ours, have proposed that interphase and mitotic chromatin are locally indistinguishable (Maeshima et al., 2010b; Joti et al., 2012; Bouchet-Marquis et al., 2006; Cremer et al., 2012). In the interphase nuclei, numerous compact chromatin domains, such as chromatin liquid drops, are already formed (Maeshima et al., 2010b; Joti et al., 2012). This is in good agreement with our finding of no significant differences in protein mobility or local nucleosome dynamics between interphase and mitotic chromatin. This is also consistent with the findings of the Langowski and Ellenberg groups, showing that dense heterochromatin regions are readily accessible to

Cell PRESS Open ACCESS

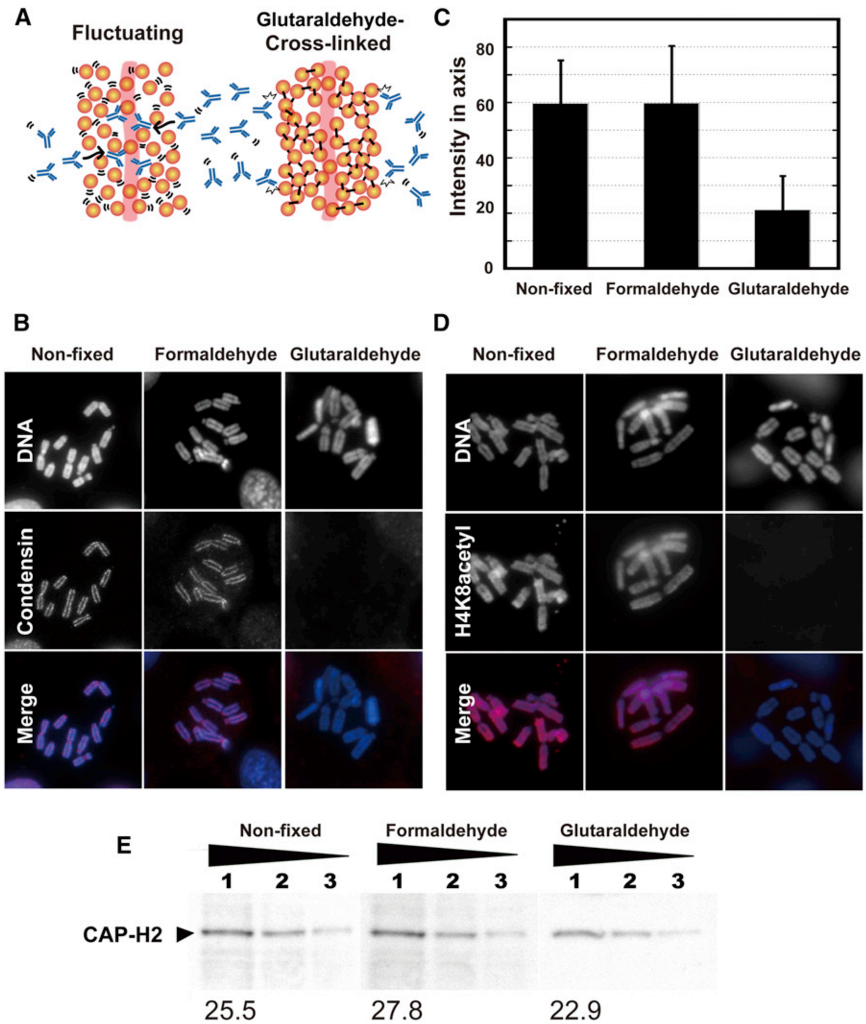

Figure 7. Tight Crosslinking of Nucleosomes Blocks Antibody Accessibility and Targeting

(A) Schematic representation of the experiment. Protein accessibility and targeting to the chromatin were examined by immunostaining with anti-CAP-H2 monoclonal antibody (CAP-H2 is a condensin II component).

(B) Signals are detected in the nonfixed and formaldehyde-fixed chromosomes (left and center columns), but not in the glutaraldehyde-fixed chromosomes (right column). Note that the diameter (molecular mass) of the antibodies is ~15 nm (~150 kDa).

(C) Intensities of the axial signals (n = 104). The intensities of the glutaraldehyde-fixed chromosomes are significantly lower than those of the other samples. Local nucleosome fluctuation was evident in living cells (Figures 5C and 5D) and formaldehyde-fixed cells (Figure S7A), but not in glutaraldehyde-fixed cells (Figure 5F). Thus, the mitotic chromatin in formaldehyde-fixed cells and nonfixed cells has similar accessibility to diffusing proteins, although glutaraldehyde-fixed cells do not (Figure 5F).

(D) Immunostaining using the H4K8-acetyl antibody. Similar results to those shown in (B) were obtained.

(E) Detection of CAP-H2 signals by western blotting of cell lysates, which were fixed on the membrane using glutaraldehyde. Increasing quantities of total-cell lysates of normal DM cells were loaded into lanes 1–3. The CAP-H2 signal values after background subtraction are shown at the bottom. Note that glutaraldehyde did not change the antibody-epitope(s) in the CAP-H2 of the condensin complex.

See also Figure S7.

diffusing proteins (Weidemann et al., 2003; Dross et al., 2009; Bancaud et al., 2009).

The compaction status of chromatin has thus far been discussed in terms of average pore size, whereby more compact chromatin has a smaller pore size and vice versa (Görisch et al., 2005; for review, see Wachsmuth et al., 2008). However, as Wedemeier et al. pointed out previously (Wedemeier et al., 2009a, 2009b), this model cannot explain why the condensin complex (~600 kDa) (Gerlich et al., 2006) and topoisomerase IIα (~340 kDa in dimer form) (Tavormina et al., 2002), which are comparable in size or larger than nucleosomes, show considerable mobility inside compact chromosomes (estimated pore size, ~10 nm). The globular head domain of condensin is as large as 21 nm (Anderson et al., 2002). Local nucleosome dynamics can overcome this problem because constant local movements and rearrangements of nucleosomes allow large protein complexes to move around inside chromosomes. Consistent with this notion, our simulations show that spheres of 21 nm can move freely in 0.5 mM of fluctuating 10 nm spheres (nucleosomes). In good agreement with our findings, lattice simulations of the polymer chain performed by the Langowski group (Wedemeier et al., 2009b; Fritsch and Langowski, 2011) suggested that a dynamic polymer network facilitates movement of large particles. In their simulations, they modeled interphase cell nuclei, which exist in rather dilute environments (Wedemeier et al., 2009b; Fritsch and Langowski, 2011), whereas we focused on more condensed chromatin environments and observed more dramatic effects.

Previous studies on chromatin dynamics have employed very large regions, such as the LacO array that encompasses 20–50 nucleosomes (Straight et al., 1996; Belmont et al., 1999; Heun et al., 2001; Vazquez et al., 2001). When the movement of such regions in living mammalian cells was measured by monitoring movement of the GFP-LacI signal bound to the LacO array (Chubb et al., 2002; Levi et al., 2005), the reported mobility of the GFP-LacI signal was ATP dependent and very slow at ~1×10^{-4} $\mu m^2/s$. Meanwhile, the local nucleosome movement we identified in the present study could be very rapid in a short time period: the apparent D values of the nucleosomes at 0–30 ms were at least ~0.032 $\mu m^2/s$ (interphase) and 0.034 $\mu m^2/s$ (mitotic chromosomes). These values are roughly 100-fold higher than the Ds of GFP-LacI signals, which represent rather large chromatin fiber regions. Thus, local nucleosome movement is distinct from that observed with these large chromatin fibers.

Recently, we suggested a polymer melt-like structure that is an irregular folding of nucleosome fibers without a 30 nm chromatin structure (Maeshima et al., 2010a; Nishino et al., 2012; Joti et al., 2012). This melt-like structure implies that the nucleosome fibers might be constantly moving and rearranging at the local level. The single-nucleosome imaging in the present study demonstrated such local nucleosome dynamics. Notably, the mean nucleosome movement for 30 ms (51 nm in the x-y plane in interphase chromatin; 59 nm in the x-y plane in mitotic chromosomes) was significantly longer than 30 nm. This finding also provides evidence that there are almost no 30 nm chromatin fibers in the majority of cells.

The local nucleosome dynamics of the polymer melt-like structure facilitates protein mobility and chromatin accessibility. This is important for many biological processes. For example, because the large protein complexes condensin and topoisomerase IIα are essential for the chromosome assembly process (for review, see Losada and Hirano, 2005; Maeshima and Eltsov, 2008), local nucleosome dynamics may contribute to their functions in the structural maintenance of chromosomes. In addition, upon scanning genome information, the dynamic local movement of nucleosomes can facilitate the movement of transcription complexes and their targeting to specific DNA sites. This advantage would also be true for many other "target searching" biological processes, such as DNA repair, replication, and recombination. Regulation of local chromatin dynamics, possibly by histone modification and/or specific proteins, would be an important aspect in the regulation of such biological processes.

EXPERIMENTAL PROCEDURES

FCS Measurement and Quantitative Analysis

Live-cell imaging was performed using an LSM510 confocal laser microscope (Carl Zeiss, Germany). LSM observations were all performed at 25°C. EGFPn (n = 1, 3, or 5) was excited at 488 nm with a CW Ar^+ laser through a water-immersion objective lens (C-Apochromat, 40×, 1.2 NA; Carl Zeiss). H2B-mRFP1 was imaged using a 543 nm laser light. To avoid bleed-through effects in double-scanning experiments, EGFP and mRFP1 were scanned independently in a multitracking mode.

FCS measurements were all performed at 25°C on a ConfoCor 2 (Carl Zeiss), as described previously (Pack et al., 2006). Excitation of EGFP was carried out at 488 nm (under 6.3 μW) by adjusting the acousto-optical tunable filter (AOTF) to the minimum level. All autocorrelation functions were measured for 10 s five times or fewer, at 2 s intervals, because the mitotic chromosome moves very slowly during the mitotic process, causing nonstationary slow fluorescent fluctuations during long measurement periods. FCS measurements of the proteins in living cells and data analysis were conducted as described previously (Pack et al., 2006). Briefly, to obtain the diffusion time, the fluorescence autocorrelation curve functions (FAFs; $G(\tau)$) of the measurements were fitted by the following one-component model with or without a triplet term:

$$G(\tau) = 1 + \frac{1}{N}\left(\frac{1}{1+\tau/\tau_D}\right)\left(\frac{1}{1+(1/s)^2(\tau/\tau_D)}\right)^{\frac{1}{2}},$$

where N is the number of molecules in detection volume, τ_D is correlation time, *w* and *z* are the width and axial length of the detection volume, respectively, and *s* is the structure parameter (*z/w)*.

Diffusion times show the following relationship to the *D*:

$$\tau_D = w^2/4D.$$

The *D* of EGFP (τ_{EGFP}) was calculated from the reported value of *D* of control Rho6G (D_{Rh6G} = 280 $\mu m^2/s$), and the measured values of the diffusion times of Rh6G (τ_{Rh6G}) and EGFP (D_{EGFP}), as follows:

$$\frac{D_{EGFP}}{D_{Rh6G}} = \frac{\tau_{Rh6G}}{\tau_{EGFP}}.$$

Note that all FAFs from the FCS measurements under our conditions were well fitted by the one-component model (Figure S2; see figure legend for details) (Pack et al., 2006). For the oligomeric EGFP molecules (monomer to pentamer) in the cells, the autocorrelation function can be fitted by the two-component model or anomalous diffusion model. Although we performed such an analysis (Pack et al., 2006), the contribution of the slower component might be small (approximately 5%). Therefore, we used the simple one-component model to extract the main component of diffusion property. The results of the fitting are shown in Figure S2.

Monte Carlo Simulation of Nucleosomes and EGFP Pentamers

All molecules were represented as hard spherical bodies. Diffusive motions of the molecules were calculated using the Metropolis Monte Carlo method without long-range potentials and hydrodynamic interactions (Morelli and ten Wolde, 2008). The diameters and *D*s of the nucleosomes (10 nm spheres) and EGFP pentamers (13 nm spheres) used in the simulations were 10.3 nm and 8.68 $\mu m^2/s$, and 12.8 nm and 7.00 $\mu m^2/s$, respectively. These values were obtained as follows: the 10 nm sphere representing a nucleosome was determined to have a volume equivalent to that of a nucleosome (Luger et al., 1997). The *D* of the 10 nm sphere was obtained using the Stokes-Einstein relation based on the diameter and *D* of EGFP monomers measured in the cytoplasm (3.80 nm and 23.5 $\mu m^2/s$, respectively). The diameter of EGFP pentamers was also obtained using the same relation from the *D* obtained by FCS measurements.

Simulations were conducted in a cubic box of 149 nm with periodic boundaries. In total, 100 spheres of 13 nm (EGFP pentamers) and 200 or 1,000 spheres of 10 nm (nucleosomes; corresponding to 0.1 or 0.5 mM, respectively) were placed randomly. A simulation is conducted by repeating the following step-by-step procedure: (1) for each particle, a displacement ($\Delta \mathbf{r}$) is drawn using pseudorandom numbers from the continuous probability density function ($P(\mathbf{r};\Delta t) = \exp[-|\mathbf{r}|^2/(4D\Delta t)]/[8(\pi D\Delta t)^{3/2}]$); (2) a putative position for the particle ($\mathbf{r}_{new} = \mathbf{r} + \Delta\mathbf{r}$) is computed, where $\mathbf{r}$ is the current position of the particle; (3) whether the particle placed at the new putative position ($\mathbf{r}_{new}$) overlaps with any other particles is checked, and if it does, the move is rejected, and the particle is placed back in the original position $\mathbf{r}$; and (4) steps 1–3 are repeated for all particles in a random order that is newly determined in every step. When all the particles are processed, the time for Δt is advanced, and the series of procedures is restarted. Results were obtained by averaging 1,000 samples from ten independent trials. The simulation time step was 1 ns. Similar results with a shorter time step (0.1 ns) confirmed the simulation convergence. The "dog on a leash" model does not allow the 10 nm spheres (nucleosomes) to displace more than a defined distance from their initial positions at t = 0 s; if such a displacement occurs, the move is rejected in step 3 above. Control simulation for single-sphere movement without molecular crowding was performed to check the numerical algorithm and to verify that the known Brownian motion of spheres is indeed recovered (Figure S3A).

Visualization of Single-Nucleosome Motion in Living Mammalian Cells

A homemade optical setup with a fluorescence microscope (TE 2000-E: Nikon) (Tani et al., 2005) was used to observe the distribution of single PA-GFP-H4 molecules expressed in DM cells. Light from a 20 mW, 488 nm, diode-pumped, solid-state laser was introduced into the microscope through an optical path installed on a vibration insulation table. Two neutral density filters and an electromagnetic shutter were placed in the optical path. Through an objective lens (100× PlanApo TIRF, NA 1.49; Nikon), DM cells grown on a glass coverslip were exposed to the excitation light. The incident angle of the laser beam to the specimen plane was chosen so as to obtain a highly inclined plane illumination (HILO system; Tokunaga et al., 2008). Collected fluorescence from the cells was focused on the electron-multiplied CCD camera (Andor Technology, UK). The observation stage was kept at a constant 37°C. For imaging of PA-GFP, interference filters were used. The length of a side of a single pixel corresponded to 40 nm on the specimen plane.

Subpixel accuracy positions of the PA-GFP dots were determined using the image-processing software PolyParticleTracker (Rogers et al., 2007). The accuracy for determining the position of fluorescent dots was estimated using the FIONA method (Thompson et al., 2002; Yildiz et al., 2003; Ober et al., 2004). With this procedure, the trajectory of each fluorescent dot was obtained. We calculated the displacement and the MSD of fluorescent nucleosomes from the tracking data (857 points from 8 cells in interphase, 844 points from 12 cells in mitosis, 37 points from 8 cells fixed with 2% glutaraldehyde, and 100 points from fluorescence beads). The originally calculated MSD was in two dimensions. To obtain the 3D value, the two-dimensional value was multiplied by 1.5 ($4Dt \rightarrow 6Dt$). Using KaleidaGraph (Synergy Software, USA), histograms of the displacement were prepared.

PA-GFP-histone H4 has some flexible regions, including the linker and histone tail, which is maximally 50 amino acid residues, corresponding to a length of ~17 nm. We observed by FCS rapid movement of free GFP in the chromosomes at 15 μm^2/s. If PA-GFP is rapidly mobile within a restricted area, like a "dog on a leash," we consider that the effect of the flexible region on the nucleosome position determination is negligible.

SUPPLEMENTAL INFORMATION

Supplemental Information includes Extended Experimental Procedures, seven figures, and three movies and can be found with this article online at http://dx.doi.org/10.1016/j.celrep.2012.11.008.

LICENSING INFORMATION

ACKNOWLEDGMENTS

We are grateful to M. Eltsov for insightful discussion and to F. Kamada, S. Tamura, and A. Watanabe for assistance. We thank T. Tachibana for preparing antibodies; H. Kimura, K. Kimura, and R.W. Dirks for materials; Y. Hiromi, Y. Taniguchi, and I. Hiratani for critical reading of the manuscript; and A. Bancaud, S. Huet, J. Ellenberg, M. Hiroshima, Y. Joti, K. Horikawa, K. Ura, T. Hirano, H. Kimura, and members of the K.M. lab for helpful discussions. This work was supported by a MEXT grant-in-aid and a CREST grant. S.H. was supported by the JSPS.

Received: March 20, 2012
Revised: September 15, 2012
Accepted: November 9, 2012
Published: December 13, 2012

REFERENCES

Abney, J.R., Cutler, B., Fillbach, M.L., Axelrod, D., and Scalettar, B.A. (1997). Chromatin dynamics in interphase nuclei and its implications for nuclear structure. J. Cell Biol. *137*, 1459–1468.

Alberts, B., Johnson, A., Lewis, J., Raff, M., Roberts, K., and Walter, P. (2008). Molecular Biology of the Cell, Fifth Edition: The Problems Book (New York: Garland Science).

Anderson, D.E., Losada, A., Erickson, H.P., and Hirano, T. (2002). Condensin and cohesin display different arm conformations with characteristic hinge angles. J. Cell Biol. *156*, 419–424.

Bancaud, A., Huet, S., Daigle, N., Mozziconacci, J., Beaudouin, J., and Ellenberg, J. (2009). Molecular crowding affects diffusion and binding of nuclear proteins in heterochromatin and reveals the fractal organization of chromatin. EMBO J. *28*, 3785–3798.

Becker, N.B., and Everaers, R. (2009). DNA nanomechanics: how proteins deform the double helix. J. Chem. Phys. *130*, 135102.

Belmont, A.S., Sedat, J.W., and Agard, D.A. (1987). A three-dimensional approach to mitotic chromosome structure: evidence for a complex hierarchical organization. J. Cell Biol. *105*, 77–92.

Belmont, A.S., Li, G., Sudlow, G., and Robinett, C. (1999). Visualization of large-scale chromatin structure and dynamics using the lac operator/lac repressor reporter system. Methods Cell Biol. *58*, 203–222.

Bouchet-Marquis, C., Dubochet, J., and Fakan, S. (2006). Cryoelectron microscopy of vitrified sections: a new challenge for the analysis of functional nuclear architecture. Histochem. Cell Biol. *125*, 43–51.

Chen, D., Dundr, M., Wang, C., Leung, A., Lamond, A., Misteli, T., and Huang, S. (2005). Condensed mitotic chromatin is accessible to transcription factors and chromatin structural proteins. J. Cell Biol. *168*, 41–54.

Chuang, C.H., and Belmont, A.S. (2007). Moving chromatin within the interphase nucleus-controlled transitions? Semin. Cell Dev. Biol. *18*, 698–706.

Chubb, J.R., Boyle, S., Perry, P., and Bickmore, W.A. (2002). Chromatin motion is constrained by association with nuclear compartments in human cells. Curr. Biol. *12*, 439–445.

Cremer, T., Markaki, Y., Hübner, B., Zunhammer, A., Strickfaden, H., Beichmanis, S., Heß, M., Schermelleh, L., Cremer, M., and Cremer, C. (2012). Chromosome territory organization within the nucleus. In Encyclopedia of Molecular Cell Biology and Molecular Medicine, R.A. Meyers, ed. (New York: Wiley-VCH Verlag GmbH).

Daban, J.R. (2003). High concentration of DNA in condensed chromatin. Biochem. Cell Biol. *81*, 91–99.

Diesinger, P.M., Kunkel, S., Langowski, J., and Heermann, D.W. (2010). Histone depletion facilitates chromatin loops on the kilobasepair scale. Biophys. J. *99*, 2995–3001.

Dross, N., Spriet, C., Zwerger, M., Müller, G., Waldeck, W., and Langowski, J. (2009). Mapping eGFP oligomer mobility in living cell nuclei. PLoS One *4*, e5041.

Dubochet, J., Adrian, M., Schultz, P., and Oudet, P. (1986). Cryo-electron microscopy of vitrified SV40 minichromosomes: the liquid drop model. EMBO J. *5*, 519–528.

Eltsov, M., Maclellan, K.M., Maeshima, K., Frangakis, A.S., and Dubochet, J. (2008). Analysis of cryo-electron microscopy images does not support the existence of 30-nm chromatin fibers in mitotic chromosomes in situ. Proc. Natl. Acad. Sci. USA *105*, 19732–19737.

Finch, J.T., and Klug, A. (1976). Solenoidal model for superstructure in chromatin. Proc. Natl. Acad. Sci. USA *73*, 1897–1901.

Fritsch, C.C., and Langowski, J. (2010). Anomalous diffusion in the interphase cell nucleus: the effect of spatial correlations of chromatin. J. Chem. Phys. *133*, 025101.

Fritsch, C.C., and Langowski, J. (2011). Chromosome dynamics, molecular crowding, and diffusion in the interphase cell nucleus: a Monte Carlo lattice simulation study. Chromosome Res. *19*, 63–81.

Fussner, E., Ching, R.W., and Bazett-Jones, D.P. (2011a). Living without 30nm chromatin fibers. Trends Biochem. Sci. *36*, 1–6.

Fussner, E., Djuric, U., Strauss, M., Hotta, A., Perez-Iratxeta, C., Lanner, F., Dilworth, F.J., Ellis, J., and Bazett-Jones, D.P. (2011b). Constitutive heterochromatin reorganization during somatic cell reprogramming. EMBO J. *30*, 1778–1789.

Gerlich, D., Hirota, T., Koch, B., Peters, J.M., and Ellenberg, J. (2006). Condensin I stabilizes chromosomes mechanically through a dynamic interaction in live cells. Curr. Biol. *16*, 333–344.

Görisch, S.M., Wachsmuth, M., Tóth, K.F., Lichter, P., and Rippe, K. (2005). Histone acetylation increases chromatin accessibility. J. Cell Sci. *118*, 5825–5834.

Griffiths, G., Burke, B., and Lucocq, L. (1993). Fine Structure Immunocytochemistry (London: Springer-Verlag).

Gross, D., and Webb, W.W. (1986). Molecular counting of low-density lipoprotein particles as individuals and small clusters on cell surfaces. Biophys. J. *49*, 901–911.

Harms, G.S., Cognet, L., Lommerse, P.H., Blab, G.A., and Schmidt, T. (2001). Autofluorescent proteins in single-molecule research: applications to live cell imaging microscopy. Biophys. J. *80*, 2396–2408.

Heun, P., Laroche, T., Shimada, K., Furrer, P., and Gasser, S.M. (2001). Chromosome dynamics in the yeast interphase nucleus. Science *294*, 2181–2186.

Hinde, E., Cardarelli, F., Digman, M.A., Kershner, A., Kimble, J., and Gratton, E. (2011). The impact of mitotic versus interphase chromatin architecture on the molecular flow of EGFP by pair correlation analysis. Biophys. J. *100*, 1829–1836.

Hirano, T. (2005). Condensins: organizing and segregating the genome. Curr. Biol. *15*, R265–R275.

Johnston, F.P., Church, R.B., and Lin, C.C. (1982). Chromosome rearrangement between the Indian muntjac and Chinese muntjac is accompanied by a delection of middle repetitive DNA. Can. J. Biochem. *60*, 497–506.

Joti, Y., Hikima, T., Nishino, Y., Kamada, F., Hihara, S., Takata, H., Ishikawa, T., and Maeshima, K. (2012). Chromosomes without a 30-nm chromatin fiber. Nucleus *3*, 404–410.

Kimura, H., and Cook, P.R. (2001). Kinetics of core histones in living human cells: little exchange of H3 and H4 and some rapid exchange of H2B. J. Cell Biol. *153*, 1341–1353.

Kornberg, R.D. (1974). Chromatin structure: a repeating unit of histones and DNA. Science *184*, 868–871.

Korolev, N., Fan, Y., Lyubartsev, A.P., and Nordenskiöld, L. (2012). Modelling chromatin structure and dynamics: status and prospects. Curr. Opin. Struct. Biol. *22*, 151–159.

Kues, T., Dickmanns, A., Lührmann, R., Peters, R., and Kubitscheck, U. (2001). High intranuclear mobility and dynamic clustering of the splicing factor U1 snRNP observed by single particle tracking. Proc. Natl. Acad. Sci. USA *98*, 12021–12026.

Levi, V., Ruan, Q., Plutz, M., Belmont, A.S., and Gratton, E. (2005). Chromatin dynamics in interphase cells revealed by tracking in a two-photon excitation microscope. Biophys. J. *89*, 4275–4285.

Lippincott-Schwartz, J., and Patterson, G.H. (2009). Photoactivatable fluorescent proteins for diffraction-limited and super-resolution imaging. Trends Cell Biol. *19*, 555–565.

Losada, A., and Hirano, T. (2005). Dynamic molecular linkers of the genome: the first decade of SMC proteins. Genes Dev. *19*, 1269–1287.

Luger, K., Mäder, A.W., Richmond, R.K., Sargent, D.F., and Richmond, T.J. (1997). Crystal structure of the nucleosome core particle at 2.8 A resolution. Nature *389*, 251–260.

Maeshima, K., and Eltsov, M. (2008). Packaging the genome: the structure of mitotic chromosomes. J. Biochem. *143*, 145–153.

Maeshima, K., Hihara, S., and Eltsov, M. (2010a). Chromatin structure: does the 30-nm fibre exist in vivo? Curr. Opin. Cell Biol. *22*, 291–297.

Maeshima, K., Hihara, S., and Takata, H. (2010b). New insight into the mitotic chromosome structure: irregular folding of nucleosome fibers without 30-nm chromatin structure. Cold Spring Harb. Symp. Quant. Biol. *75*, 439–444.

Manders, E.M., Kimura, H., and Cook, P.R. (1999). Direct imaging of DNA in living cells reveals the dynamics of chromosome formation. J. Cell Biol. *144*, 813–821.

Marshall, W.F., Straight, A., Marko, J.F., Swedlow, J., Dernburg, A., Belmont, A., Murray, A.W., Agard, D.A., and Sedat, J.W. (1997). Interphase chromosomes undergo constrained diffusional motion in living cells. Curr. Biol. *7*, 930–939.

McDowall, A.W., Smith, J.M., and Dubochet, J. (1986). Cryo-electron microscopy of vitrified chromosomes in situ. EMBO J. *5*, 1395–1402.

McNally, J.G. (2011). Foreword. Biophysics in chromatin structure and nuclear dynamics. Chromosome Res. *19*, 1–3.

Metropolis, N., Rosenbluth, A.W., Rosenbluth, M.N., Teller, A.H., and Teller, E. (1953). Equation of state calculations by fast computing machines. J. Chem. Physiol. *21*, 1087–1092.

Morelli, M.J., and ten Wolde, P.R. (2008). Reaction Brownian dynamics and the effect of spatial fluctuations on the gain of a push-pull network. J. Chem. Phys. *129*, 054112.

Mütze, J., Ohrt, T., and Schwille, P. (2011). Fluorescence correlation spectroscopy in vivo. Laser Photon. Rev. *5*, 52–67.

Nishino, Y., Eltsov, M., Joti, Y., Ito, K., Takata, H., Takahashi, Y., Hihara, S., Frangakis, A.S., Imamoto, N., Ishikawa, T., and Maeshima, K. (2012). Human mitotic chromosomes consist predominantly of irregularly folded nucleosome fibres without a 30-nm chromatin structure. EMBO J. *31*, 1644–1653.

Ober, R.J., Ram, S., and Ward, E.S. (2004). Localization accuracy in single-molecule microscopy. Biophys. J. *86*, 1185–1200.

Olins, A.L., and Olins, D.E. (1974). Spheroid chromatin units (v bodies). Science *183*, 330–332.

Pack, C., Saito, K., Tamura, M., and Kinjo, M. (2006). Microenvironment and effect of energy depletion in the nucleus analyzed by mobility of multiple oligomeric EGFPs. Biophys. J. *91*, 3921–3936.

Perišić, O., Collepardo-Guevara, R., and Schlick, T. (2010). Modeling studies of chromatin fiber structure as a function of DNA linker length. J. Mol. Biol. *403*, 777–802.

Rigler, R., and Elson, E.L. (2001). Fluorescence Correlation Spectroscopy: Theory and Applications (Berlin: Springer-Verlag).

Rogers, S.S., Waigh, T.A., Zhao, X., and Lu, J.R. (2007). Precise particle tracking against a complicated background: polynomial fitting with Gaussian weight. Phys. Biol. *4*, 220–227.

Sako, Y., Minoghchi, S., and Yanagida, T. (2000). Single-molecule imaging of EGFR signalling on the surface of living cells. Nat. Cell Biol. *2*, 168–172.

Sandin, S., Ofverstedt, L.G., Wikström, A.C., Wrange, O., and Skoglund, U. (2004). Structure and flexibility of individual immunoglobulin G molecules in solution. Structure *12*, 409–415.

Schlick, T., Hayes, J., and Grigoryev, S. (2012). Toward convergence of experimental studies and theoretical modeling of the chromatin fiber. J. Biol. Chem. *287*, 5183–5191.

Schütz, G.J., Kada, G., Pastushenko, V.P., and Schindler, H. (2000). Properties of lipid microdomains in a muscle cell membrane visualized by single molecule microscopy. EMBO J. *19*, 892–901.

Sedat, J., and Manuelidis, L. (1978). A direct approach to the structure of eukaryotic chromosomes. Cold Spring Harb. Symp. Quant. Biol. *42*, 331–350.

Sheetz, M.P., Turney, S., Qian, H., and Elson, E.L. (1989). Nanometre-level analysis demonstrates that lipid flow does not drive membrane glycoprotein movements. Nature *340*, 284–288.

Soutoglou, E., and Misteli, T. (2007). Mobility and immobility of chromatin in transcription and genome stability. Curr. Opin. Genet. Dev. *17*, 435–442.

Straight, A.F., Belmont, A.S., Robinett, C.C., and Murray, A.W. (1996). GFP tagging of budding yeast chromosomes reveals that protein-protein interactions can mediate sister chromatid cohesion. Curr. Biol. *6*, 1599–1608.

Tani, T., Miyamoto, Y., Fujimori, K.E., Taguchi, T., Yanagida, T., Sako, Y., and Harada, Y. (2005). Trafficking of a ligand-receptor complex on the growth cones as an essential step for the uptake of nerve growth factor at the distal end of the axon: a single-molecule analysis. J. Neurosci. *25*, 2181–2191.

Tavormina, P.A., Côme, M.G., Hudson, J.R., Mo, Y.Y., Beck, W.T., and Gorbsky, G.J. (2002). Rapid exchange of mammalian topoisomerase II alpha at kinetochores and chromosome arms in mitosis. J. Cell Biol. *158*, 23–29.

Thompson, R.E., Larson, D.R., and Webb, W.W. (2002). Precise nanometer localization analysis for individual fluorescent probes. Biophys. J. *82*, 2775–2783.

Tokunaga, M., Imamoto, N., and Sakata-Sogawa, K. (2008). Highly inclined thin illumination enables clear single-molecule imaging in cells. Nat. Methods *5*, 159–161.

Vazquez, J., Belmont, A.S., and Sedat, J.W. (2001). Multiple regimes of constrained chromosome motion are regulated in the interphase Drosophila nucleus. Curr. Biol. *11*, 1227–1239.

Vologodskii, A., and Rybenkov, V.V. (2009). Simulation of DNA catenanes. Phys. Chem. Chem. Phys. *11*, 10543–10552.

Wachsmuth, M., Caudron-Herger, M., and Rippe, K. (2008). Genome organization: balancing stability and plasticity. Biochim. Biophys. Acta *1783*, 2061–2079.

Wedemeier, A., Merlitz, H., and Langowski, J. (2009a). Anomalous diffusion in the presence of mobile obstacles. Europhys. Lett. *88*, 38004.

Wedemeier, A., Merlitz, H., Wu, C.X., and Langowski, J. (2009b). How proteins squeeze through polymer networks: a Cartesian lattice study. J. Chem. Physiol. *131*, 064905.

Weidemann, T., Wachsmuth, M., Knoch, T.A., Müller, G., Waldeck, W., and Langowski, J. (2003). Counting nucleosomes in living cells with a combination of fluorescence correlation spectroscopy and confocal imaging. J. Mol. Biol. *334*, 229–240.

Wiesmeijer, K., Krouwels, I.M., Tanke, H.J., and Dirks, R.W. (2008). Chromatin movement visualized with photoactivable GFP-labeled histone H4. Differentiation *76*, 83–90.

Woodcock, C.L., Safer, J.P., and Stanchfield, J.E. (1976). Structural repeating units in chromatin. I. Evidence for their general occurrence. Exp. Cell Res. *97*, 101–110.

Woodcock, C.L., Frado, L.L., and Rattner, J.B. (1984). The higher-order structure of chromatin: evidence for a helical ribbon arrangement. J. Cell Biol. *99*, 42–52.

Yildiz, A., Forkey, J.N., McKinney, S.A., Ha, T., Goldman, Y.E., and Selvin, P.R. (2003). Myosin V walks hand-over-hand: single fluorophore imaging with 1.5-nm localization. Science *300*, 2061–2065.

Zink, D., Sadoni, N., and Stelzer, E. (2003). Visualizing chromatin and chromosomes in living cells. Methods *29*, 42–50.